A Mechanically Rollable Reflectarray With Beam-Scanning Capabilities

ANTONIO J. RUBIO (Graduate Student Member, IEEE), **ABDUL-SATTAR KADDOUR** (Member, IEEE), **AND STAVROS V. GEORGAKOPOULOS** (Senior Member, IEEE)

Department of Electrical and Computer Engineering, Florida International University, Miami, FL 33199, USA

CORRESPONDING AUTHOR: A. J. RUBIO (e-mail: antrubio@fiu.edu)

ABSTRACT A novel 1-D beam-steerable reflectarray antenna (RA) is proposed for the K_u-band. The RA aperture consists of 24×48 variable size square patch elements printed on a flexible plastic substrate. The aperture is wrapped around two cylinders to create a $12\lambda \times 12\lambda$ illumination window at the operating frequency of 14 GHz. Beam-steering is achieved by mechanically rolling the aperture. To mitigate antenna pattern degradation, an aperture phase distribution optimization technique is presented. The performance of this RA system is studied analytically using array theory. The effects of aperture size and unit-cell size are also discussed. The performance of the proposed RA is validated using simulations and measurements. The results illustrate that our design achieves 1-D beam-steering from $-21°$ to $+21°$ in the elevation plane while maintaining towards the broadside direction a maximum realized gain of 25.1 dBi. In this beam-scanning range, the gain variation is less than 1.5 dB, beamwidth variation is less than 1.6°, and the side lobe level is maintained below -15 dB. In summary, the main advantage of our design is its ability to steer its high gain beam without using complicated feed networks or complex mechanical systems. Such antennas are especially needed in SmallSat and space applications.

INDEX TERMS Mechanical beam-steering, beam-scanning, reflectarray antenna, deployable antenna, small satellite, space applications.

I. INTRODUCTION

THE REDUCTION in volume and mass of small satellites (SmallSats) has enabled more efficient and robust missions in space [1], [2], which has led to exponential growth in the number of SmallSats launched each year. The communications networks proposed by OneWeb, SpaceX, and Telesat alone are expected to deploy at least 8,000 SmallSats in lower earth orbit by the year 2024 [3]. However, for most satellite applications, it is challenging to meet the communication system requirements due to the small size of SmallSats. Specifically, in such platforms, the large attenuation losses of transmitted signals must be overcome using systems that meet the space constraints of SmallSat buses. Therefore, high gain antennas (HGA) have been proposed to achieve longer transmission distances with higher efficiency thereby minimizing the volume and mass of the needed power systems. Furthermore, a key

requirement in advanced SmallSat applications is beam-scanning [4]. However, traditional beam-scanning HGAs are not practical for SmallSat applications given the power and space constraints. Therefore, current research is focusing on developing compact/deployable beam-scanning HGAs for space applications [4], [5], [6]. The proposed solutions are generally based on traditional HGA technologies, such as, parabolic reflector antennas [7], [8], [9], phased array antennas [10], [11], [12], [13], and reflectarray antennas (RAs) [14], [15], [16], [17], [18]. Compared to the parabolic reflector and phased array antennas, RAs provide highly directive and versatile beams while maintaining low mass, low fabrication cost, and low complexity [19], [20]. Also, RAs have recently demonstrated the ability to achieve pattern reconfigurability [21]. However, current reconfigurable RA designs suffer from various limitations including lossy and complex DC biasing networks that drive reconfigurable

elements [22], or inefficient mechanical systems [23]. In this paper, we present a novel 1-D beam-steering RA system that uses a simple and efficient scrolling mechanism to steer its beam along a single cut plane. Our approach uses a flexible RA aperture that is wrapped around two columns, which can rotate, causing the aperture to roll, as shown in Fig. 1. The aperture is first synthesized to steer its main beam towards the broadside direction, as shown in Fig. 1(b). Then, the aperture is rolled as shown in Fig. 1(a) and Fig. 1(c), thereby defocusing the RA feed antenna causing the main beam to scan towards the direction of rotation.

Our novel rollable RA was first studied in [24], but only a preliminary study to validate the phase optimization procedure was presented. In this work, we present the theoretical background of our optimization procedure, and analytically investigate how the aperture layout and unit-cell size affect the beam-scanning performance of our design. Then, a rollable RA is synthesized to operate in the K_u-band, and it is simulated using ANSYS HFSS® full-wave simulation software. A prototype is then fabricated and measured to validate our design. An accurate characterization of the flexible substrate is performed by conducting parametric simulations and unit-cell measurements. Finally, the effectiveness of our proposed optimization procedure is validated. The rollable RA prototype achieves 42° of lateral beam-scanning while maintaining a maximum realized gain of 25.1 dBi with a 1.5 dB variation. Our rollable RA uses a simple and low profile mechanism, thereby eliminating the need for complicated, bulky, and inefficient feed networks or mechanical systems. This makes our design an ideal candidate for reconfigurable HGA applications in compact spaces, such as, SmallSats or tactical equipment.

The paper is organized as follows: Section II provides a brief background on SmallSat RAs and reconfigurable RA technologies. Section III details our optimization procedure for realizing the element phase distribution across the aperture. Section IV presents the synthesis of the RA system, the fabrication details of our prototype, and our simulation and measurement results. Finally, Section V provides our conclusions and highlights the key findings of our work.

II. BACKGROUND

Recently, the viability of deployable RAs on SmallSat systems has been demonstrated with NASA missions for deep space [25], and lower earth orbit [26] applications. However, these missions relied on either a reaction wheel system or an Attitude Determination and Control System (ADCS) to meet the pointing accuracy requirements of the antennas. This method of beam-scanning adds significant cost, mass, and complexity to the overall mission, and reduces the lifespan of SmallSats. Furthermore, some missions involve instrumentation that precludes the adjustment of spacecrafts' pitch, roll, and yaw [27]. Alternatively, RAs with beam-scanning capability provide unique advantages to distributed swarm antenna arrays [28], satellite clusters [29], and SmallSat constellations [30], [31].
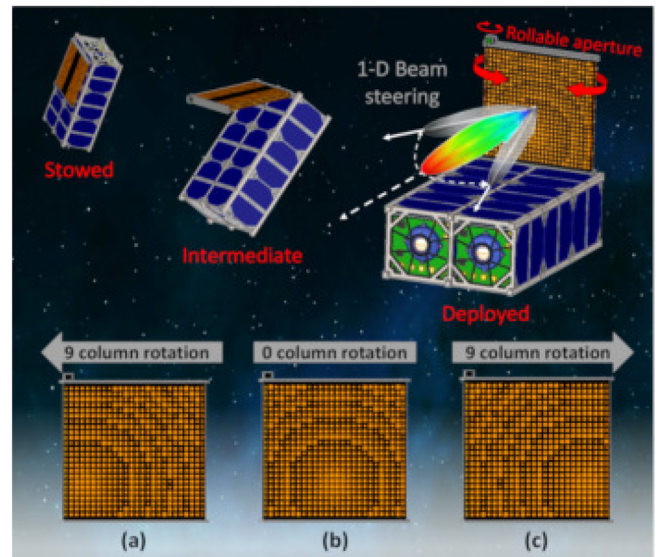

FIGURE 1. Proposed rollable reflectarray on a 6U CubeSat with the RA aperture rolled (a) 9 columns to the left, (b) centered, and (c) 9 columns to the right.

Beam-scanning RAs are typically realized using either phase-tuning, or feed-tuning. In each of these approaches, the phase distribution, $\phi_{RP}(x_i, y_i)$, across the RA aperture is tuned to steer the main beam towards the desired direction, as shown in (1):

$$\phi_{RP}(x_i, y_i) = \phi_{PP}(x_i, y_i) - k_0 R_i \tag{1}$$

where ϕ_{PP} and $-k_0 R_i$ are the progressive phase and spatial phase delay of the ith unit-cell of the aperture, respectively [21]. The phase-tuning technique achieves pattern reconfigurability by tuning the ϕ_{PP} of each unit-cell. Proposed approaches include the use of electromechanical components [32], [33], [34], electronic components [35], [36], [37], [38], optical components [39], [40], [41], and smart materials [42], [43], [44]. Phase-tuning approaches for RAs can achieve high-speed beam-scanning but require complicated DC biasing networks, and materials, which in turn increase the cost of RAs and make them less competitive compared to phased array technologies [27], [45], [46], [47].

Alternatively, the feed-tuning technique tunes the spatial phase delay of the unit-cells. This is accomplished by changing the distance, R_i, between the unit-cells and the feed antenna phase center. Proposed approaches include single feed systems that mechanically tune R_i [48], [49], [50], or multiple feed systems that create discrete values of R_i [51], [52], [53]. Multiple feed systems are not well suited for SmallSat applications since they add significant mass to the spacecraft and require individual feed networks and complicated deployment mechanisms. Also, current single feed systems are not ideal for SmallSats since they require inefficient mechanical systems to physically move either the feed antenna or the aperture. Furthermore, the large sweeping movements of feed tuning approaches

cover a large volume of space, which could obstruct other instrumentation. Recently, alternative approaches have been proposed [54], [55], [56], which tune R_i by folding the RA aperture instead. However, the drawback of this approach is its limited beam-scanning angle. In [57], Legay et al., proposed a reconfigurable reflectarray that scrolls through several radiating apertures printed on a single flexible substrate. However, their aperture design is bulky and does not provide continuous beam-scanning capability.

The benefits of our rollable RA design are that we can achieve high gain and continuous beam-scanning with a low-profile, simple, and efficient aperture rolling mechanism. The trade-offs to such a simple design are that the direction of beam-scanning is limited to the axis of aperture rotation and the scanning speed is limited to the speed of rotation. However, 2D beam-scanning could be achieved by tilting the RA system along an orthogonal axis with a simple tilting mechanism, like a motor and hinge. It should be noted that tilting the aperture on an orthogonal axis changes the incidence angle on the array which could lead to degradation of the radiation pattern [20], but these effects could be mitigated by characterizing the elements under different angles of incidence and using a lookup table during aperture synthesis. Also, there are several SmallSat applications that do not require high-speed beam-scanning. Such applications can benefit from the beam-steering capabilities of our design. For example, our proposed design can use its beam-steering capabilities to: (1) satisfy the pointing accuracy requirements of satellite relay stations, (2) adjust the scanning area of remote sensing satellites, or (3) tune the focal point of a distributed swarm antenna array.

III. DESIGN METHODOLOGY AND THEORETICAL STUDY

In this section, our proposed synthesis process for our rollable beam-scanning aperture is described. Also, analytical studies are presented here to characterize performance of our proposed RA and demonstrate the effectiveness of our optimized synthesis process.

A. BEAM-SCANNING BY DEFOCUSING THE FEED ANTENNA

It has been shown that reflector antennas can achieve beam-scanning by defocusing the feed antenna [58], [59], [60]. The effects of defocusing an RA are presented in [50], where it was found that the main beam can be scanned by laterally shifting the position of the feed. Alternatively, the RA can be defocused by axially shifting the aperture while maintaining the feed position fixed. Fig. 2(a) shows an RA, which is synthesized to point its beam towards the broadside direction. This RA is centered on the coordinate system with origin O_0, which is shown in red. Fig. 2(b) shows the geometric configuration of the RA after the aperture is shifted along the $-x$-axis a distance d_i, so that it is centered on the relative coordinate system with origin O_i, which is shown in black. This lateral shift creates a similar defocusing effect as presented in [50], only in this case there
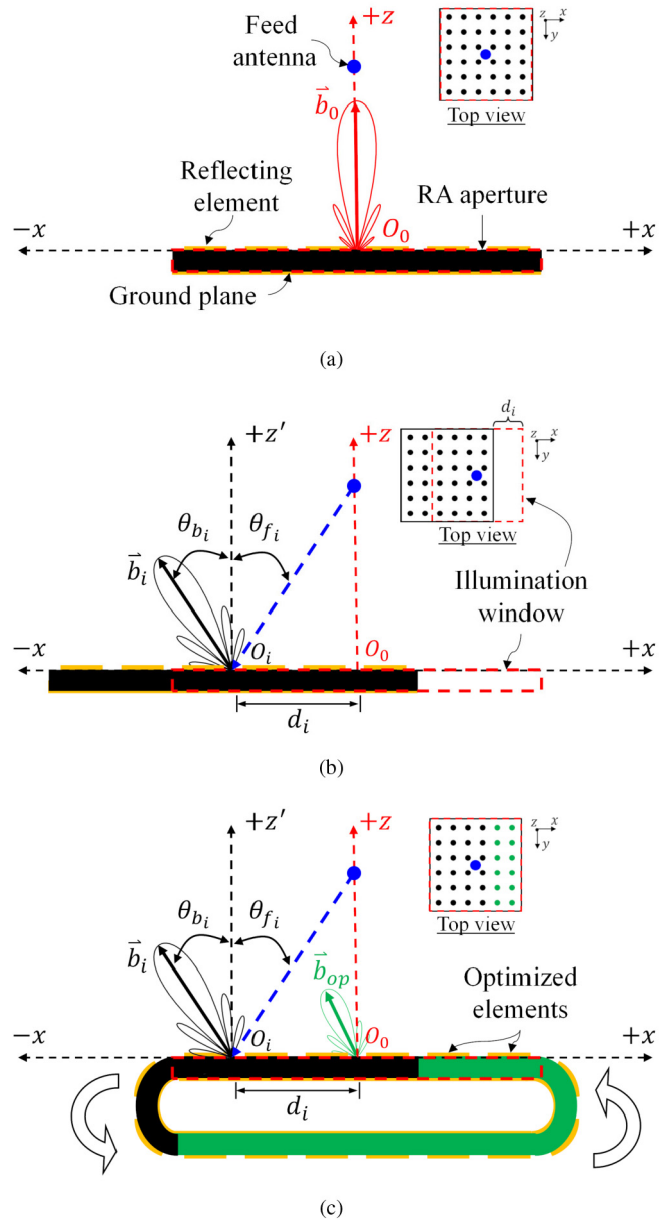

FIGURE 2. Effects of defocusing the feed antenna of an RA by laterally shifting the aperture: (a) initially the RA is synthesized to steer the main beam towards the broadside direction and the feed antenna is focused, (b) the RA aperture is shifted laterally, defocusing the feed antenna and scanning the beam towards $\vec{b}_i$, and (c) the proposed rollable RA design introduces optimized elements to reinforce the scanned beam.

is no secondary mechanism that re-aligns the feed antenna pattern with the center of the aperture. The defocusing angle, θ_{f_i}, caused by the shift creates a proportional beam-scanning angle, θ_{b_i}, that directs the main beam along $\vec{b}_i$, as shown in Fig. 2(b). However, laterally shifting the aperture causes the same problems as laterally shifting the feed antenna: (1) reduction in effective aperture size by a factor of $\cos \theta_{f_i}$, (2) reduction of aperture efficiency from increased spillover and non-uniform aperture illumination, and (3) introduction of phase errors due to the change in spatial phase delay of the elements [50].
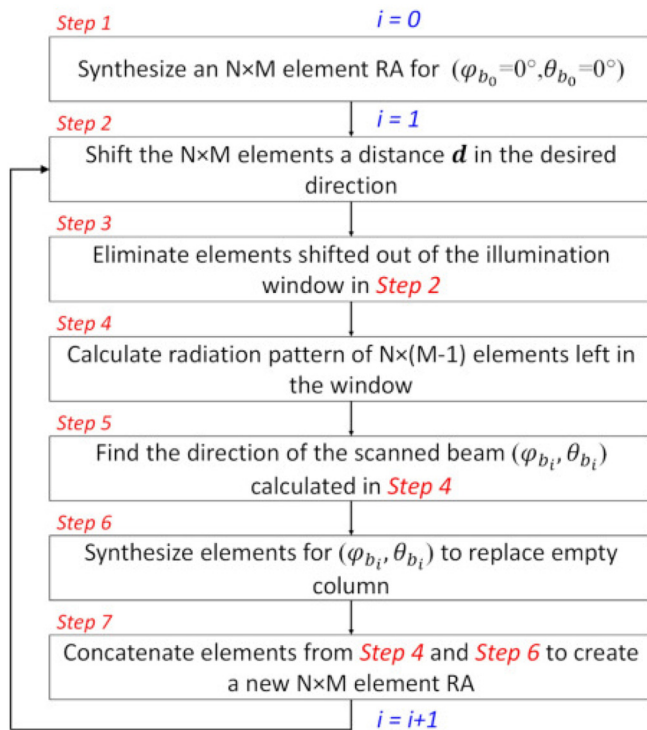
FIGURE 3. Flowchart of our proposed optimization process for our rollable RA.

The flowchart contains:

Step 1 — i = 0: Synthesize an N×M element RA for ($\varphi_{b_0}=0°, \theta_{b_0}=0°$)

Step 2 — i = 1: Shift the N×M elements a distance **d** in the desired direction

Step 3: Eliminate elements shifted out of the illumination window in Step 2

Step 4: Calculate radiation pattern of N×(M−1) elements left in the window

Step 5: Find the direction of the scanned beam ($\varphi_{b_i}, \theta_{b_i}$) calculated in Step 4

Step 6: Synthesize elements for ($\varphi_{b_i}, \theta_{b_i}$) to replace empty column

Step 7: Concatenate elements from Step 4 and Step 6 to create a new N×M element RA — i = i+1

B. APERTURE PHASE DISTRIBUTION OPTIMIZATION

To minimize all these effects, we propose a rollable RA design, as shown in Fig. 2(c). As the aperture rolls, the elements rolled out of the illumination window are out of the sight of the feed antenna. Simultaneously, optimized elements, shown in green, are rolled in the illumination window. The optimized elements serve three purposes: (1) maintain the effective aperture size constant, (2) maintain high aperture efficiency by minimizing spill over and maintaining uniform amplitude tapering, and (3) minimizing total phase errors of the illumination window. To minimize the total phase errors, the reflection phase of the elements rolled in the illumination window are optimized to radiate in the direction of the scanned beam, $\vec{b}_{op} = \vec{b}_i$, as shown in Fig. 2(c).

The flowchart for our proposed phase distribution optimization process is shown in Fig. 3. In Step 1, the phase distribution of a $N \times M$ element RA is synthesized to radiate a main beam towards the broadside direction ($\phi = 0°, \theta = 0°$) using the ray-tracing method [20]. Then, in Step 2, the RA elements are rolled laterally a distance d, which is equal to the width of one element column, to the first rolling position, $i = 1$. Next, in Step 3, the column of elements shifted out of the illumination window is eliminated to simulate it being rolled behind the ground plane and out of sight of the feed antenna. In Step 4, the radiation pattern of the remaining $N \times (M - 1)$ element array is calculated using array theory [20]. In Step 5, the direction of the main beam, (ϕ_{b_i}, θ_{b_i}), from the radiation pattern calculated in Step 4 is found. In Step 6, a column vector of N elements, positioned in the empty column created by the roll in Step 2, is synthesized

to radiate towards direction (ϕ_{b_i}, θ_{b_i}). In Step 7, the column of elements obtained from Step 6 are concatenated with the $N \times (M - 1)$ elements generated in Step 3 to form a new $N \times M$ phase distribution in the illumination window. Then, Steps 2 through 7 are repeated on the new $N \times M$ phase array to generate an optimized column of elements for the second rolling position, $i = 2$. This process is repeated for the number of column rotations required to achieve the desired beam-scanning angle. The result of the procedure is a $N \times (M + 2i)$ phase distribution matrix.

To illustrate how our optimization process works, we examine an example aperture with dimensions $10\lambda \times 10\lambda$ with 0.5λ inter-element spacing. Fig. 4 shows the 20×20 element matrix for this aperture at three different rolling positions $i = 0$, 5, and 10. In Fig. 4(a), the RA aperture is shown in the reference position, $i = 0$, where the elements shown in black are synthesized in Step 1 to scan the main beam towards the broadside. After 5 iterations of the optimization procedure in the $-x$-direction, the RA is at the fifth rolling position, $i = 5$, resulting in 5 columns of optimized elements in the illumination window, shown in green in Fig. 4(b). After 10 iterations, the RA is at the tenth rolling position, $i = 10$, and there are 10 optimized columns on the illumination window, as shown in Fig. 4(c). If the optimization process is stopped after 10 column rotations, $i = 10$, in both directions, the resulting aperture phase distribution would consist of a 20×40 phase matrix, where the first 10 columns of the matrix are optimized for rolling in the $+x$-direction, the next 20 columns contain the phase distribution for the reference position, $i = 0$, and the last 10 columns are optimized for rolling in the $-x$-direction.

C. CHARACTERIZING THE ROLLABLE RA PERFORMANCE ANALYTICALLY

To study the performance of our proposed RA, we consider a square aperture with length A discretized by a square lattice with unit-cell length d, as shown in Fig. 4(a). In this setup, the feed is assumed to be a point source positioned at the broadside direction at a distance $f/A = 0.8$, where f is the focal distance. The feed antenna pattern is defined by $\cos^{2q}(\theta)$ [20], with a q-factor of 4.25. Four different aperture sizes are considered in our analysis: $A = 10\lambda$, 20λ, 30λ, and 40λ. For each of the these apertures, four unit-cell sizes, d, are analyzed: $d = 0.3\lambda$, 0.4λ, 0.5λ, and 0.6λ. Specifically, for each combination of the aperture and unit-cell size, a rollable aperture is synthesized using the procedure described in Section III-B. In total, 16 rollable RA apertures were synthesized. Then, the performance of each aperture is characterized by calculating the radiation pattern for each rolling position, i, analytically using array theory [20]. The results of our analytical study are shown in Fig. 5. Specifically, the directivity and beam direction are plotted versus the rolling position, i, in the $-x$-direction until the grating lobes of the rollable RA overtake the main beam (i.e., SLL = 0). The results for rolling in the $+x$-direction are symmetric; therefore, they are omitted for brevity. From the results, it
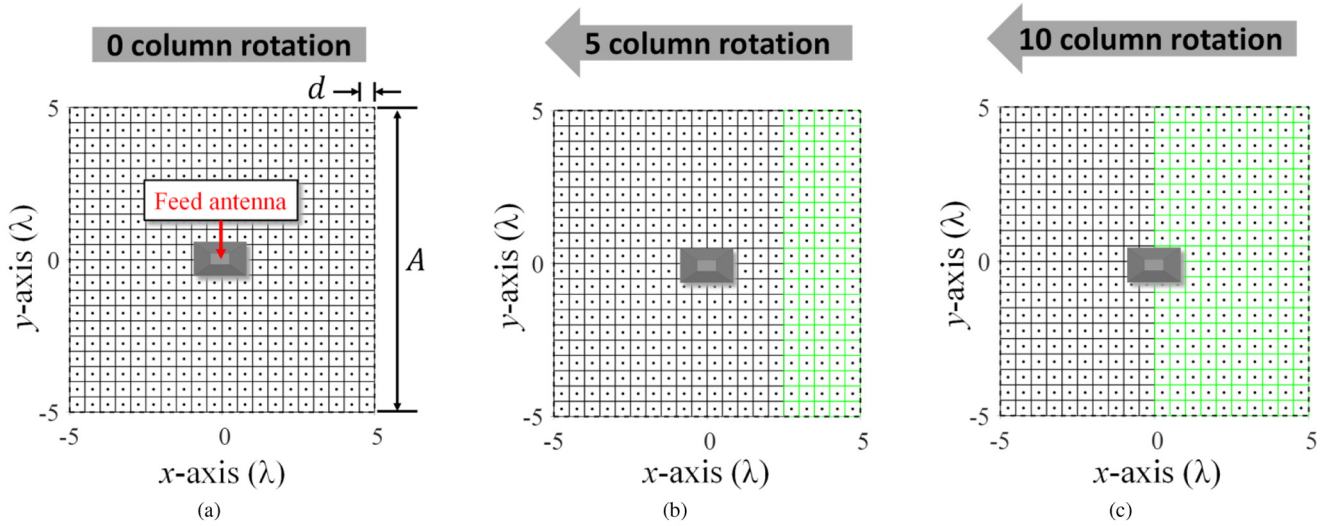
FIGURE 4. Configuration for an example aperture $A \times A$ ($A = 10\lambda$ and inter-element spacing $d = 0.5\lambda$) with the optimized elements according to our proposed process (shown in green) for different rolling positions, i, towards the $-x$-direction: (a) $i = 0$, (b) $i = 5$, and (c) $i = 10$.
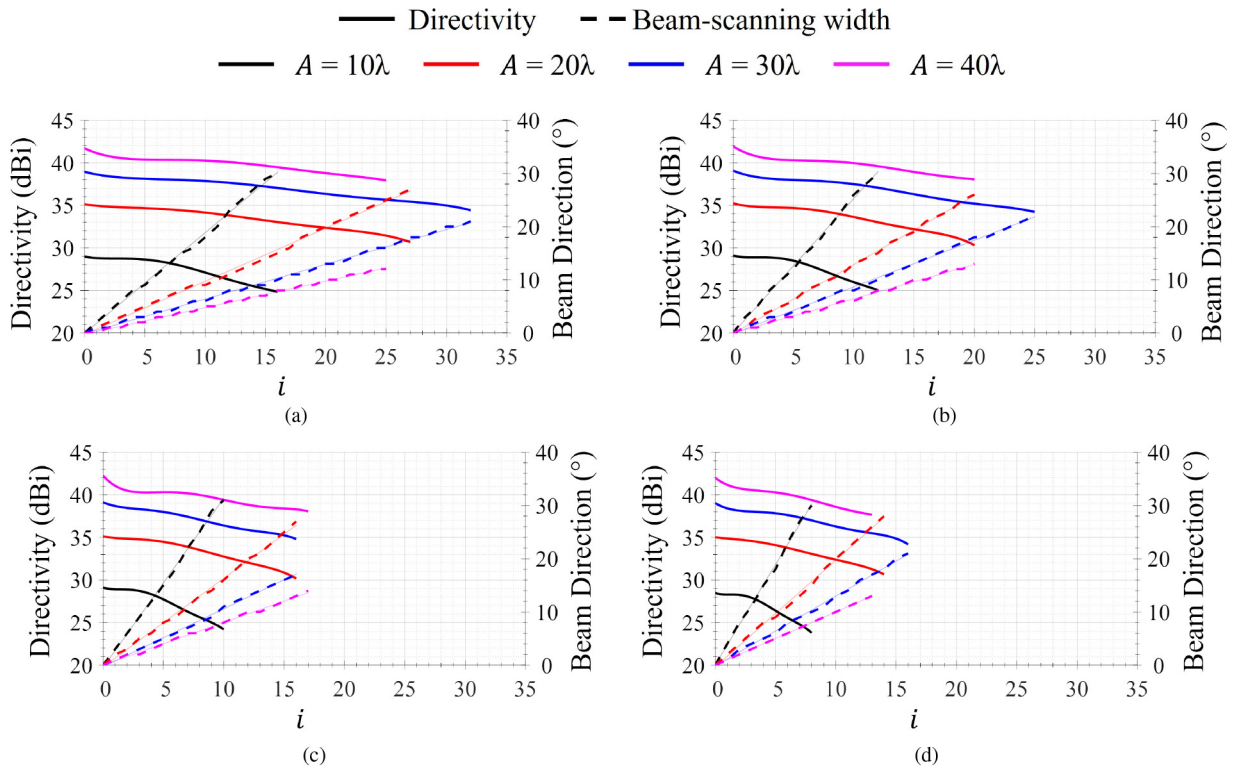

FIGURE 5. Directivity and main beam direction vs. rolling position, i, calculated analytically for four different aperture sizes, A, and unit-cell sizes: (a) $d = 0.3\lambda$, (b) $d = 0.4\lambda$, (c) $d = 0.5\lambda$, and (d) $d = 0.6\lambda$.

can be seen that for all the cases beam direction is a relatively linear function with respect to the rolling position, i. In other words, for any given case of aperture and unit-cell size, the beam direction at any i can be approximated by a line with slope equal to the scanning precision (SP), which is the degrees of beam-scanning achieved per wavelength distance of translation (°/λ). The maximum deviation of beam direction from the linear approximation was $< 2°$ for all cases.

1) EFFECT OF APERTURE SIZE ON BEAM-SCANNING PERFORMANCE

The theoretical maximum directivity of a reflecting aperture with area, A_{ap}, is given by $D_0 = 4\pi A_{ap}/\lambda^2$, where λ is the wavelength at the frequency of operation. When the side length of the aperture, A, increases, the maximum directivity (D_0) of the aperture increases. However, increasing A reduces the scanning range due to a faster gain

degradation. For example, in Fig. 4(c) it can be seen that for a maximum allowable directivity variance of 1.5 dB, an aperture with $A = 10\lambda$ can achieve a scan angle of $33.4°$, while a $A = 40\lambda$ aperture can only achieve $1.2°$. The maximum scanning angle is inversely proportional to A because larger apertures have more reflecting elements that introduce larger cumulative phase errors when the columns of the aperture are rolled. In turn, these larger cumulative phase errors generate side lobes and degrade the main beam. Therefore, increasing the aperture size to achieve higher directivity comes at the expense of smaller beam-scanning angle.

Furthermore, our results show that SP is inversely proportional to the aperture size, A. Specifically, as A increases, the focal distance, f, should increase to maintain high aperture efficiency [56]. Therefore, for larger apertures, a smaller defocusing angle $\theta_f = \arctan(d/f)$ is created after each column roll. For example, Fig. 4(c) shows that an aperture with size $A = 10\lambda$ or $A = 40\lambda$ can steer the beam with a SP of $6.21°/\lambda$ or $1.71°/\lambda$, respectively. Therefore, a larger aperture requires a higher number of rolled columns to reach a specific beam-scanning angle. It should be mentioned that SP is a function of the feed position and can be increased by using a less directive feed antenna which would reduce the f/A ratio.

2) EFFECT OF UNIT-CELL SIZE ON BEAM-SCANNING PERFORMANCE

In our design, the unit-cell size, d, determines the rolling step of the aperture. Therefore, the effects of d on the performance of the rollable RA were also investigated. Our results illustrate that d has negligible effect on the performance of our rollable RA. Specifically, Fig. 4 shows that for a given aperture size, A, the beam-scanning angle and SP remain relatively constant for variable d at the -1.5, -3, and -4 dB directivity levels. This demonstrates that our optimization process can be applied to any design regardless of unit-cell size. Notably, for a fixed size aperture, the inter-element spacing of an RA is determined by the unit-cell size, and the amount of mutual coupling between the elements of an RA depends on its inter-element spacing [20], [61], [62], [63], [64]. Our study was conducted analytically using array theory; therefore, the effects of mutual coupling were not included, but should be considered in the design process.

This analysis shows that our novel phase synthesis technique achieves good beam-scanning performance for different combinations of A and d. However, it should be mentioned that the rollable RA aperture is a platform that can support any phase synthesis technique used for translating apertures. For example, a phase synthesis approach for a translating aperture is presented in [65]. Similar designs using a bi-focal approach were presented in [66] and [67]. These techniques, among others, could be implemented on the rollable RA aperture to achieve the desired beam-scanning performance.
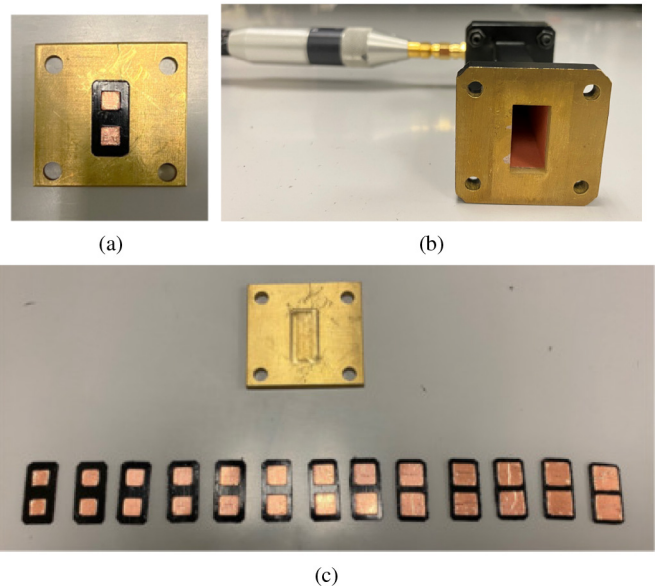

FIGURE 6. WR-75 waveguide measurement setup showing: (a) unit-cell element in the measurement flange, (b) waveguide connected to the VNA, and (c) measurement flange and element batch #1.

IV. EXAMPLE ROLLABLE RA DESIGN

Our optimization procedure is used here to design a rollable beam-scanning RA. Specifically, in this section, we present the unit-cell characterization for our RA as well as our simulation and measurement results.

A. UNIT-CELL CHARACTERIZATION

Our proposed rollable aperture must use a flexible substrate that can wrap around two rotating columns. Apart from being flexible, the substrate must possess appropriate dielectric material properties to achieve adequate phase range and acceptable losses. Therefore, by carefully reviewing different materials, a sheet of 0.762mm thick low-density polyethylene (LDPE) was chosen for our application. Even though the properties of this material were reported by the manufacturer (i.e., $\epsilon_r = 2.3$ and $tan\delta = 0.001$ at microwave frequencies), it was not clear what the material properties are at our design's operational frequency of 14 GHz. To accurately design our proposed RA and minimize any phase errors that would occur from not accurately knowing the material properties of our substrate, we chose to perform a material characterization. A waveguide measurement setup was established using a VNA and a WR-75 waveguide to replicate an infinite array scenario, as shown in Fig. 6. A custom flange was fabricated out of brass to fit the WR-75 waveguide. Reflecting unit-cells with different sizes of square patches were fabricated and measured. Specifically, three batches of unit-cells with different sizes were made to characterize how the dielectric properties of our substrate vary across the material sample that we purchased. Each batch consisted of 13 different sizes of unit-cells, ranging from 5 to 8mm at 0.25mm increments. The unit-cells were made by applying copper tape with conductive adhesive to the top and bottom surfaces of
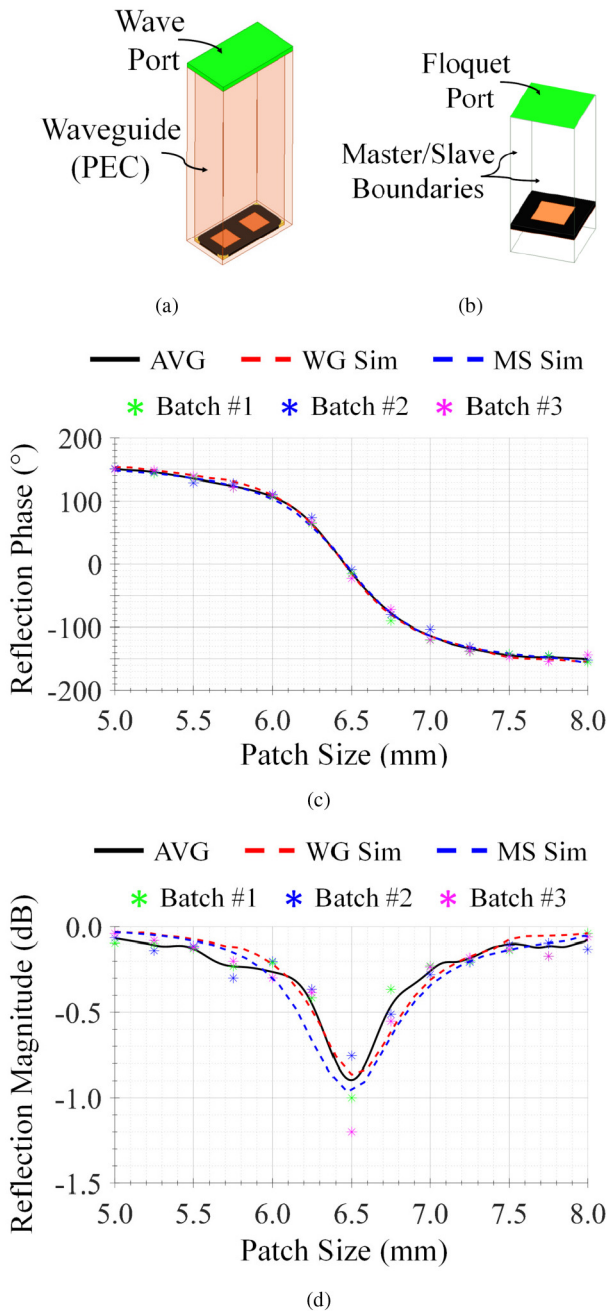
(a)   (b)

(c)

(d)

FIGURE 7. Comparison between simulated and measured data of our unit-cells at the operating frequency (14 GHz): (a) Waveguide simulation setup (WG Sim), (b) Master/slave boundary simulation setup (MS Sim), (c) reflection phase (S-curve), and (d) reflection magnitude.

the LDPE material. The patches were created on the top surface with a CNC cutting machine and the excess tape was removed. Then, the reflection phase and magnitude of each unit-cell were measured and recorded. The average curves of the reflection phase and magnitude of the three batches were calculated and fitted using a polynomial function.

Then, the measured unit-cells were simulated on ANSYS HFSS by modeling a waveguide with PEC boundaries fed by a wave port, as shown in Fig. 7(a). The dielectric properties of the material were found numerically by

Illumination Window
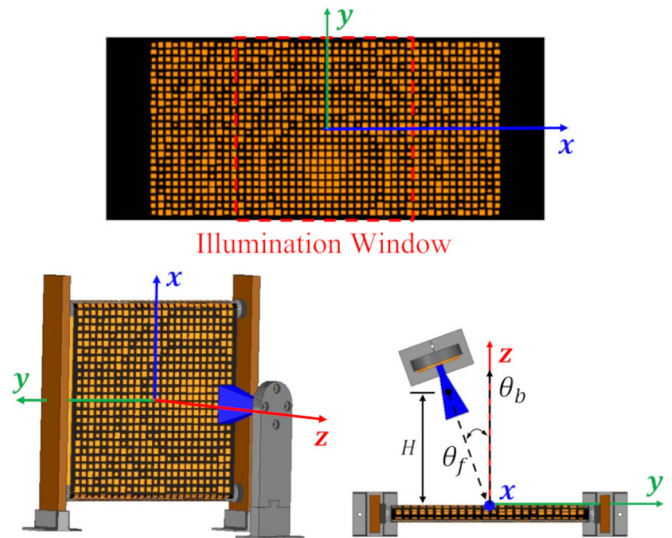
FIGURE 8. CAD model of the rollable RA prototype used in our full-wave simulations.

running parametric simulations until the results of the simulation matched our measurements. Through this process we arrived at these properties for our substrate: $\epsilon_r = 2.1$ and $tan\delta = 0.01$. Finally, the material properties were simulated with a single unit-cell using master/slave boundaries, as shown in Fig. 7(b). The simulated results for the waveguide (WG Sim) and master/slave boundary (MS Sim) models are compared to the measured data and the polynomial fitting function of the average data of the three measured batches (AVG) in Figs. 7(c) and 7(d). The excellent comparison of the simulated and measured data validates the material properties that we calculated following our process. Also, Figs. 7(c) and 7(d) show that our unit-cell achieves a phase range of 300.4° and a maximum reflection loss of 0.9 dB, which are both sufficient for our rollable RA design.

B. ROLLABLE RA SYNTHESIS, PROTOTYPING, AND MEASUREMENT

After characterizing the material properties of our flexible substrate, we proceeded to synthesize our rollable RA at 14 GHz. Specifically, our design has an illumination window of $12\lambda \times 12\lambda$ and uses 0.5λ square unit-cells (i.e., $A = 12\lambda$, $d = 0.5\lambda$). The aperture phase distribution of our RA was synthesized using our optimization process and was designed to accommodate a maximum of 12-column rolls in either direction. Therefore, the total RA aperture size is 24×48 elements. A linearly polarized MVG SH2000 horn antenna was used as the feed. Its radiation pattern was measured and its maximum gain was 12.7 dBi at 14 GHz (i.e., q-factor $= 4.25$). The optimal feed position occurred at $f/A = 0.75$. This was calculated considering a feed offset of 20°, to reduce feed blockage, and it corresponds to a maximum aperture efficiency of 70%.
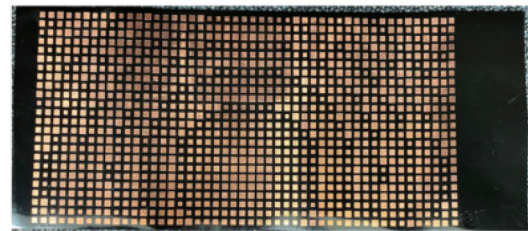
Our RA design was then modeled and simulated using ANSYS HFSS, as shown in Fig. 8. The RA is excited by a

TABLE 1. Gain budget.

Parameter	Value (dBi)
Maximum Directivity ($D = 4\pi A/\lambda^2$)	**32.6**
Feed Loss	
Spillover	-0.80
Illumination	-0.81
Impedance Mismatch	-0.11
Feed Blockage	-0.45
Material Loss	
Dielectric	-0.89
Conductor	-0.04
Fabrication Loss	
Patch Quantization ($500\mu m$)	-1.40
Machining Tolerance ($250\mu m$)	-0.12
RMS Surface Error (1mm)	-1.04
Quadratic Bow Surface Error (2mm)	-1.50
Measurement Setup Loss	
Feed Offset Angle Misalignment ($\pm 5°$)	-0.18
Polarization Misalignment ($\pm 5°$)	-0.11
Feed Height Misalignment ($\pm 2mm$)	-0.22
Total Loss	**-7.67**
Predicted Gain	**24.9**
Predicted Aperture Efficiency	**17.1%**

FIGURE 9. Rollable RA prototype: the flexible aperture fabricated with reflecting elements printed on the (a) top side and a ground plane on the (b) bottom side, then placed in the (c) measurement setup.

linked far-field source whose radiation pattern is the imported measurements of the SH2000 horn antenna. A total of 25 simulations were performed, one for each rolling position. The simulation setup considered ideal conditions to reduce the computational load. These ideal conditions reduced the required computing time and memory by 96% and 86%, respectively, saving 915 hours of total computing time. To estimate the gain penalty imposed by deviations from the ideal simulation setup, an extensive tolerance analysis was performed. The effects of feed blockage, conductor losses, machining tolerances, surface roughness, aperture bowing, and alignment errors were accounted for by conducting parametric simulations. Table 1 lists the sources of loss and shows that for the worst-case scenario of fabrication and misalignment errors, the estimated gain is 24.9 dBi and the estimated aperture efficiency is 17.1%.
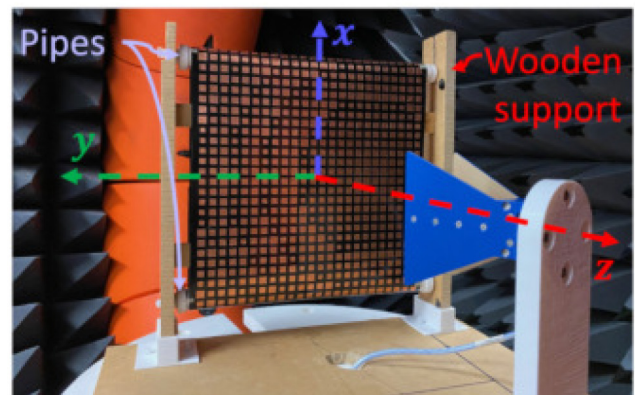
A prototype of our RA design was fabricated to validate its performance. Specifically, the aperture was fabricated using a CNC cutting technique. First, a layer of copper tape (which has conductive adhesive) was applied to the top and bottom surfaces of a $700 \times 300 \times 0.762$ mm³ sheet of LDPE with a press. Then, the 24×48 elements array of variable size patches was etched into the top layer with a precision CNC cutting machine, the Silhouette Cameo 4, which was found to have a machining tolerance of $250\mu m$. Then, the ground plane was etched into the bottom layer using the same CNC cutting technique. Figs. 9(a) and 9(b) show our manufactured RA aperture. To create our rollable design, we sewed the ends of the aperture and re-enforced this connection with epoxy. Due to space limitations of our antenna chamber, a structure was designed to hold the aperture upright and roll vertically, as shown in Fig. 9(c). The flexible aperture was then wrapped around two pipes and tension was applied to create a flatter surface. However, approximately 1-2mm of quadratic bowing on the aperture was exhibited due to the low elasticity of the material. This bowing accounted for the largest source of loss (1.5 dB) which was determined through full wave simulation and measurement of an equivalent square aperture held flat by adhering it to a rigid plastic sheet. The performance of the proposed rollable RA could be significantly improved by using materials or manufacturing techniques that minimize aperture bowing. Notably, our manufacturing method was chosen due to our available equipment, low-cost material, simplicity, and adequate fabrication tolerances to demonstrate the rollable beam-scanning concept. However, this prototype is not optimized for space applications. A space bound aperture should consider the effects of several environmental and material factors, such as, temperature gradients, solar radiation, material stresses, and expected life cycle.
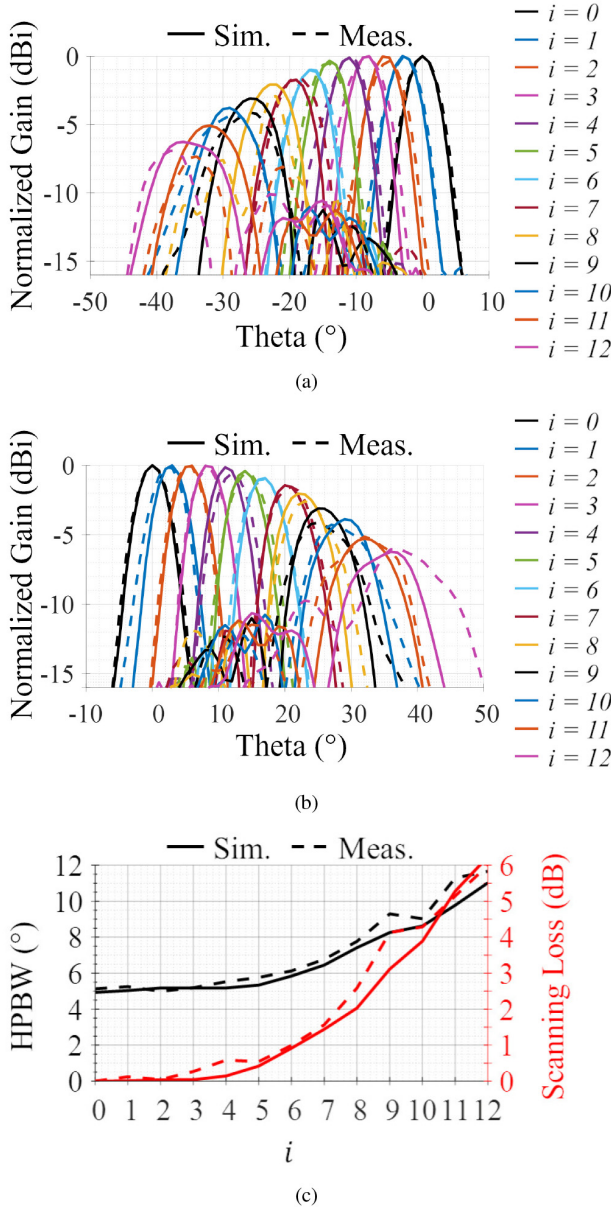
TABLE 2. Results of simulations and prototype measurements.

	Realized Gain (dBi)	η_{ap} (%)	SP (°/λ)	-1.5 dB Level		-3 dB Level		-4 dB Level	
				BSW (°)	SLL (dB)	BSW(°)	SLL (dB)	BSW(°)	SLL (dB)
Predicted	24.9	17.1	2.8	20	-16.2	23	-9.4	26	-7.4
Measurements	25.1	17.8	2.9	21	-16.3	23	-9.4	25	-7.0

a η_{ap} is the aperture efficiency.
b SP is the scanning precision.
c BSW is the beam-scanning width.
d SLL is the side lobe level.

(a)

(b)

(c)

FIGURE 10. Elevation plane cuts ($\phi = 0°$) of the co-pol realized gain pattern for rolling positions, i, in the (a) $-x$-direction, and (b) $+x$-direction. In (c), the HPBW (black) and Scanning Losses (red) are presented as a function of i.

The measurements of our RA were conducted in an MVG StarLab near-field measurement system. The different rolling positions were realized by rotating the aperture manually. However, faster and more precise rotation can be achieved by using motors. Figs. 10(a) and 10(b) show the simulated and measured xz-plane co-pol normalized gain patterns for the RA rolling towards the $-x$ and $+x$ directions, respectively. These results show good agreement between the simulations and the measurements. Specifically, the maximum predicted and measured realized gain are 24.9 and 25.1 dBi, respectively. It is also seen that the measured gain is higher than the predicted gain which indicates that the errors in the measurement setup and fabrication process were lower than the most conservative estimate. This resulted in maximum predicted and measured aperture efficiency (η_{ap}) of 17.1% and 17.8%, respectively. The maximum deviation between the predicted and measured gain for all beam directions is 0.2 dB, and the average deviation is only 0.09 dB. The maximum deviation between the simulated and measured beam direction is only 1.8°. This deviation is due to phase errors from the machining tolerance and alignment errors due to the manual rolling of the aperture. Notably, our prototyped design achieved 42° of lateral beam-scanning while maintaining a maximum gain deviation of only 1.5 dB over the entire scanning range. A summary of the measured and simulated performance of our RA design is shown in Table 2.

V. CONCLUSION

In this work, a novel rollable RA with beam-scanning capabilities was presented. Specifically, beam-scanning is achieved by defocusing the reflecting elements of the aperture as it rolls. Also, a phase distribution optimization process was proposed to reduce the phase errors and achieve optimal performance. Simulations and measurements were used to characterize our RA design and they exhibited good agreement. Our prototyped design achieved realized gain of 25.1 dBi and 42° of continuous lateral beam-scanning with a gain deviation of only 1.5 dB, while the SLL was maintained below -15 dB. Therefore, our proposed RA provides high directivity and beam-scanning capabilities using a simple, low mass, low profile, and efficient design, which makes it ideal for SmallSat applications.

REFERENCES

[1] J. R. Kopacz, R. Herschitz, and J. Roney, "Small satellites an overview and assessment," *Acta Astronautica*, vol. 170, pp. 93–105, May 2020.
[2] G. Curzi, D. Modenini, and P. Tortora, "Large constellations of small satellites: A survey of near future challenges and missions," *Aerospace*, vol. 7, no. 9, p. 133, 2020.
[3] I. Del Portillo, B. G. Cameron, and E. F. Crawley, "A technical comparison of three low earth orbit satellite constellation systems to provide global broadband," *Acta Astronautica*, vol. 159, pp. 123–135, Jun. 2019.
[4] S. Gao, Y. Rahmat-Samii, R. E. Hodges, and X.-X. Yang, "Advanced antennas for small satellites," *Proc. IEEE*, vol. 106, no. 3, pp. 391–403, Mar. 2018.

[5] S. Rao, M. Tang, and C.-C. Hsu, "Reconfigurable antenna system for satellite communications," in *Proc. IEEE Antennas Propag. Soc. Int. Symp.*, 2007, pp. 3157–3160, doi: 10.1109/APS.2007.4396206.

[6] Z. N. Chen, X. Qing, X. Tang, W. E. I. Liu, and R. Xu, "Phased array metantennas for satellite communications," *IEEE Commun. Mag.*, vol. 60, no. 1, pp. 46–50, Jan. 2022, doi: 10.1109/MCOM.001.2100538.

[7] I. L. Vilenko, A. K. Tobolev, A. V. Shishlov, Y. V. Krivosheev, M. S. Uhm, and S. H. Yun, "Millimeter wave reflector antenna with wide angle mechanical beam scanning," in *Proc. Int. Conf. Eng. Telecommun. (En T)*, 2021, pp. 1–4, doi: 10.1109/EnT50460.2021.9681792.

[8] X. Zhu, B. Zhang, and K. Huang "A K/Ka-band dielectric and metallic 3D printed aperture shared multibeam parabolic reflector antenna for satellite communication," *Int. J. RF Microw. Comput.-Aided Eng.*, vol. 30, no. 7, 2020, Art. no. e22216.

[9] S. Shao, S. Song, M. Xu, and W. Jiang, "Mechanically reconfigurable reflector for future smart space antenna application," *Smart Mater. Struct.*, vol. 27, no. 9, 2018, Art. no. 95014.

[10] A. Jacomb-Hood and E. Lier, "Multibeam active phased arrays for communications satellites," *IEEE Microw. Mag.*, vol. 1, no. 4, pp. 40–47, Dec. 2000.

[11] G. Buttazzoni, M. Comisso, A. Cuttin, M. Fragiacomo, R. Vescovo, and R. V. Gatti, "Reconfigurable phased antenna array for extending cubesat operations to Ka-band: Design and feasibility," *Acta Astronautica*, vol. 137, pp. 114–121, Aug. 2017.

[12] N. Haider, A. G. Yarovoy, and A. G. Roederer, "*L/S*-band frequency reconfigurable multiscale phased array antenna with wide angle scanning," *IEEE Trans. Antennas Propag.*, vol. 65, no. 9, pp. 4519–4528, Sep. 2017, doi: 10.1109/TAP.2017.2722685.

[13] A. T. Muriel-Barrado, J. Calatayud-Maeso, A. Rodríguez-Gallego, P. Sánchez-Olivares, J. M. Fernández-González, and M. Sierra-Pérez, "Evaluation of a planar reconfigurable phased array antenna driven by a multi-channel beamforming module at Ka band," *IEEE Access*, vol. 9, pp. 63752–63766, 2021, doi: 10.1109/ACCESS.2021.3075060.

[14] E. Baladi, M. Y. Xu, N. Faria, J. Nicholls, and S. V. Hum, "Dual-band circularly polarized fully reconfigurable reflectarray antenna for satellite applications in the ku-band," *IEEE Trans. Antennas Propag.*, vol. 69, no. 12, pp. 8387–8396, Dec. 2021, doi: 10.1109/TAP.2021.3090577.

[15] C. A. Velez, A.-S. Kaddour, C. Ynchausti, L. L. Howell, S. P. Magleby, and S. V. Georgakopoulos, "Deployable and reconfigurable Miura-Ori reflectarray for mission-flexible satellite applications," in *Proc. IEEE Texas Symp. Wireless Microw. Circuits Syst. (WMCS)*, 2021, pp. 1–6, doi: 10.1109/WMCS52222.2021.9493295.

[16] J. S. Roper and A. F. Peterson, "Design of circularly polarized mechanically reconfigurable reflectarrays for satellite communications and power transfer," in *Proc. IEEE Int. Conf. Wireless Space Extreme Environ. (WiSEE)*, 2021, pp. 1–6, doi: 10.1109/WiSEE50203.2021.9613838.

[17] Z. Wang et al., "1 bit electronically reconfigurable folded reflectarray antenna based on p-i-n diodes for wide-angle beam-scanning applications," *IEEE Trans. Antennas Propag.*, vol. 68, no. 9, pp. 6806–6810, Sep. 2020, doi: 10.1109/TAP.2020.2975265.

[18] I.-J. Nam, S. Lee, and D. Kim, "Miniaturized beam reconfigurable reflectarray antenna with wide 3-D beam coverage," *IEEE Trans. Antennas Propag.*, vol. 70, no. 4, pp. 2613–2622, Apr. 2022, doi: 10.1109/TAP.2021.3083732.

[19] J. Huang and J. A. Encinar, *Reflectarray Antennas*, vol. 30. Hoboken, NJ, USA: Wiley, 2007.

[20] P. Nayeri, F. Yang, and A. Z. Elsherbeni, *Reflectarray Antennas: Theory, Designs, and Applications*. Hoboken, NJ, USA: Wiley, 2018.

[21] P. Nayeri, F. Yang, and A. Z. Elsherbeni, "Beam-scanning reflectarray antennas: A technical overview and state of the art," *IEEE Antennas Propag. Mag.*, vol. 57, no. 4, pp. 32–47, Aug. 2015, doi: 10.1109/MAP.2015.2453883.

[22] J.-M. Baracco, P. Ratajczak, P. Brachat, J.-M. Fargeas, and G. Toso, "Ka-band reconfigurable reflectarrays using varactor technology for space applications: A proposed design," *IEEE Antennas Propag. Mag.*, vol. 64, no. 1, pp. 27–38, Feb. 2022, doi: 10.1109/MAP.2021.3133502.

[23] M. Mirhamed et al., "Mechanically reconfigurable, beam-scanning reflectarray and transmitarray antennas: A review," *Appl. Sci.*, vol. 11, no. 15, p. 6890, 2021.

[24] A.-S. Kaddour and S. V. Georgakopoulos, "A beam-steerable rollable reflectarray," in *Proc. IEEE Int. Symp. Antennas Propag. North Amer. Radio Sci. Meeting*, 2020, pp. 545–546, doi: 10.1109/IEEECONF35879.2020.9330191.

[25] R. E. Hodges, N. Chahat, D. J. Hoppe, and J. D. Vacchione, "A deployable high-gain antenna bound for Mars: Developing a new folded-panel reflectarray for the first cubesat mission to Mars," *IEEE Antennas Propag. Mag.*, vol. 59, no. 2, pp. 39–49, Apr. 2017.

[26] R. E. Hodges et al., "The ISARA mission-flight demonstration of a high gain Ka-band antenna for 100Mbps telecom," in *Proc. 32nd Annu. AIAA/USU Conf. Small Satellites*, San Diego, CA, USA, Aug. 2018, pp. 1–6.

[27] F. Davarian et al., "Improving small satellite communications in deep space—A review of the existing systems and technologies with recommendations for improvement. Part I: Direct to Earth links and smallsat telecommunications equipment," *IEEE Aerosp. Electron. Syst. Mag.*, vol. 35, no. 7, pp. 8–25, Jul. 2020, doi: 10.1109/MAES.2020.2980918.

[28] M. B. Quadrelli, R. Hodges, V. Vilnrotter, S. Bandyopadhyay, F. Tassy, and S. Bevilacqua, "Distributed swarm antenna arrays for deep space applications," in *Proc. IEEE Aerosp. Conf.*, Mar. 2019, pp. 1–15.

[29] N. Saeed, A. Elzanaty, H. Almorad, H. Dahrouj, T. Y. Al-Naffouri, and M.-S. Alouini, "CubeSat communications: Recent advances and future challenges," *IEEE Commun. Surveys Tuts.*, vol. 22, no. 3, pp. 1839–1862, 3rd Quart., 2020, doi: 10.1109/COMST.2020.2990499.

[30] Z. Qu, G. Zhang, H. Cao, and J. Xie, "LEO satellite constellation for Internet of Things," *IEEE Access*, vol. 5, pp. 18391–18401, 2017, doi: 10.1109/ACCESS.2017.2735988.

[31] I. Leyva-Mayorga et al., "LEO small-satellite constellations for 5G and beyond-5G communications," *IEEE Access*, vol. 8, pp. 184955–184964, 2020, doi: 10.1109/ACCESS.2020.3029620.

[32] H. Legay, B. Pinte, M. Charrier, A. Ziaei, E. Girard, and R. Gillard, "A steerable reflectarray antenna with MEMS controls," in *Proc. IEEE Int. Symp. Phased Array Syst. Technol.*, Boston, MA, USA, 2003, pp. 494–499.

[33] V. F. Fusco, "Mechanical beam scanning reflectarray," *IEEE Trans. Antennas Propag.*, vol. 53, no. 11, pp. 3842–3844, Nov. 2005.

[34] X. Yang et al., "A broadband high-efficiency reconfigurable reflectarray antenna using mechanically rotational elements," *IEEE Trans. Antennas Propag.*, vol. 65, no. 8, pp. 3959–3966, Aug. 2017, doi: 10.1109/TAP.2017.2708079.

[35] S. V. Hum, M. Okoniewski, and R. J. Davies, "Realizing an electronically tunable reflectarray using varactor diode-tuned elements," *IEEE Microw. Wireless Compon. Lett.*, vol. 15, no. 6, pp. 422–424, Jun. 2005.

[36] M. M. Tahseen, T. A. Denidni, and A. A. Kishk, "Low-loss compact re-configurable reflectarray element," in *Proc. IEEE Int. Symp. Antennas Propag. USNC/URSI Nat. Radio Sci. Meeting*, 2018, pp. 475–476, doi: 10.1109/APUSNCURSINRSM.2018.8608542.

[37] E. Carrasco, M. Barba, and J. A. Encinar, "X-band reflectarray antenna with switching-beam using PIN diodes and gathered elements," *IEEE Trans. Antennas Propag.*, vol. 60, no. 12, pp. 5700–5708, Dec. 2012, doi: 10.1109/TAP.2012.2208612.

[38] H. Zhang, X. Chen, Z. Wang, Y. Ge, and J. Pu, "A 1-bit electronically reconfigurable reflectarray antenna in X band," *IEEE Access*, vol. 7, pp. 66567–66575, 2019, doi: 10.1109/ACCESS.2019.2918231.

[39] M. R. Chaharmir, J. Shaker, M. Cuhaci, and A.-R. Sebak, "Novel photonically-controlled reflectarray antenna," *IEEE Trans. Antennas Propag.*, vol. 54, no. 4, pp. 1134–1141, Apr. 2006, doi: 10.1109/TAP.2006.872644.

[40] J. Shaker, M. R. Chaharmir, M. Cuhaci, and A. Ittipiboon, "Reflectarray research at the communications research centre Canada," *IEEE Antennas Propag. Mag.*, vol. 50, no. 4, pp. 31–52, Aug. 2008, doi: 10.1109/MAP.2008.4653661.

[41] G. Boreman, E. Braunstein, J. Ginn, T. Haberfelde, and A. Hawkins, "Dynamic reflectarray technology for electro-optical sensors," UCF Patent 685, 2012. [Online]. Available: https://stars.library.ucf.edu/patents/685

[42] S. Bildik, S. Dieter, C. Fritzsch, W. Menzel, and R. Jakoby, "Reconfigurable folded reflectarray antenna based upon liquid crystal technology," *IEEE Trans. Antennas Propag.*, vol. 63, no. 1, pp. 122–132, Jan. 2015, doi: 10.1109/TAP.2014.2367491.

[43] M. Bozorgi and M. Rafaei-Booket, "Metallic array on a biased ferrite substrate as a reconfigurable reflectarray antenna," in *Proc. 9th Int. Symp. Telecommun. (IST)*, 2018, pp. 80–85, doi: 10.1109/ISTEL.2018.8661066.

[44] M. Tamagnone and J. R. Mosig, "Theoretical limits on the efficiency of reconfigurable and nonreciprocal graphene antennas," *IEEE Antennas Wireless Propag. Lett.*, vol. 15, pp. 1549–1552, 2016, doi: 10.1109/LAWP.2016.2521835.

[45] R. J. Mailloux, *Phased Array Antenna Handbook*, 2nd ed. Norwood, MA, USA: Artech House, 2005.

[46] G. M. Rebeiz and L. M. Paulsen, "Advances in low-cost phased arrays using silicon technologies," in *Proc. IEEE Int. Symp. Antennas Propag. USNC/URSI Nat. Radio Sci. Meeting*, 2017, pp. 1035–1036.

[47] A. Naqvi and S. Lim, "Review of recent phased arrays for millimeter-wave wireless communication," *Sensors*, vol. 18, no. 10, p. 3194, 2018.

[48] G.-B. Wu, S.-W. Qu, and S. Yang, "Wide-angle beam-scanning reflectarray with mechanical steering," *IEEE Trans. Antennas Propag.*, vol. 66, no. 1, pp. 172–181, Jan. 2018, doi: 10.1109/TAP.2017.2775282.

[49] M. I. Abbasi, M. H. Dahri, M. H. Jamaluddin, N. Seman, M. R. Kamarudin, and N. H. Sulaiman, "Millimeter Wave beam steering reflectarray antenna based on mechanical rotation of array," *IEEE Access*, vol. 7, pp. 145685–145691, 2019, doi: 10.1109/ACCESS.2019.2945318.

[50] S. R. Rengarajan, "Scanning and defocusing characteristics of microstrip reflectarrays," *IEEE Antennas Wireless Propag. Lett.*, vol. 9, pp. 163–166, 2010, doi: 10.1109/LAWP.2010.2045217.

[51] A. Z. Elsherbeni, P. Nayeri, and F. Yang, "Reflectarray antennas for space applications," in *Proc. IEEE Int. Conf. Ultra-Wideband*, 2012, pp. 362–365, doi: 10.1109/ICUWB.2012.6340389.

[52] M. Zawadzki, S. R. Rengarajan, and R. E. Hodges, "The design of H- and V-pol waveguide slot array feeds for a scanned offset dual-polarized reflectarray," in *Proc. IEEE Int. Antennas Propag. Symp.*, vol. 2B. Washington, DC, USA, Jul. 2005, pp. 417–420.

[53] M. Arrebola, J. A. Encinar, and M. Barba, "Multifed printed reflectarray with three simultaneous shaped beams for LMDS central station antenna," *IEEE Trans. Antennas Propag.*, vol. 56, no. 6, pp. 1518–1527, Jun. 2008, doi: 10.1109/TAP.2008.923360.

[54] A. S. Kaddour et al., "A foldable and reconfigurable monolithic reflectarray for space applications," *IEEE Access*, vol. 8, pp. 219355–219366, 2020.

[55] A.-S. Kaddour, C. A. Velez, and S. V. Georgakopoulos, "A deployable and reconfigurable origami reflectarray based on the Miura-Ori pattern," in *Proc. IEEE Int. Symp. Antennas Propag. North Amer. Radio Sci. Meeting*, 2020, pp. 91–92, doi: 10.1109/IEEECONF35879.2020.9329994.

[56] A. S. Kaddour and S. V. Georgakopoulos, "Reconfigurable rotational reflectarrays," U.S. Patent 10 910 713, Feb. 2, 2021.

[57] H. Legay et al., "Recent developments on reflectarray antennas at Thales Alenia Space," in *Proc. 3rd Eur. Conf. Antennas Propag.*, Berlin, Germany, 2009, pp. 2515–2519.

[58] C. A. Balanis, *Antenna Theory: Analysis and Design*. Hoboken, NJ, USA: Wiley, 2015.

[59] Y. Rahmat-Samii, "Reflector antennas," in *Antenna Handbook*. Boston, MA, USA: Springer, 1988. pp. 949–1072.

[60] J. W. M. Baars, *The Paraboloidal Reflector Antenna in Radio Astronomy and Communication*, vol. 348. New York, NY, USA: Springer, 2007.

[61] A. Yu, F. Yang, A. Z. Elsherbeni, J. Huang, and Y. Rahmat-Samii, "Aperture efficiency analysis of reflectarray antennas," *Microw. Opt. Technol. Lett.*, vol. 52, no. 2, pp. 364–372, 2010.

[62] F. Venneri, S. Costanzo, and G. Di Massa, "Wideband aperture-coupled reflectarrays with reduced inter-element spacing," in *Proc. IEEE Antennas Propag. Soc. Int. Symp.*, 2008, pp. 1–4, doi: 10.1109/APS.2008.4619759.

[63] E. Almajali, D. A. McNamara, J. Shaker, and M. R. Chaharmir, "Observations on the performance of reflectarrays with reduced inter-element spacings," in *Proc. IEEE Int. Symp. Antennas Propag. (APSURSI)*, 2011, pp. 369–372, doi: 10.1109/APS.2011.5996720.

[64] S. Costanzo and F. Venneri, "Miniaturized fractal reflectarray element using fixed-size patch," *IEEE Antennas Wireless Propag. Lett.*, vol. 13, pp. 1437–1440, 2014, doi: 10.1109/LAWP.2014.2341032.

[65] E. B. Lima, S. A. Matos, J. R. Costa, C. A. Fernandes, and N. J. G. Fonseca, "Circular polarization wide-angle beam steering at Ka-band by in-plane translation of a plate lens antenna," *IEEE Trans. Antennas Propag.*, vol. 63, no. 12, pp. 5443–5455, Dec. 2015, doi: 10.1109/TAP.2015.2484419.

[66] S. A. Matos, E. B. Lima, J. R. Costa, C. A. Fernandes, and N. J. G. Fonseca, "Design of a 40 dBi planar bifocal lens for mechanical beam steering at Ka-band," in *Proc. 10th Eur. Conf. Antennas Propag. (EuCAP)*, 2016, pp. 1–4, doi: 10.1109/EuCAP.2016.7481442.

[67] P. Nayeri, F. Yang, and A. Z. Elsherbeni, "Bifocal design and aperture phase optimizations of reflectarray antennas for wide-angle beam scanning performance," *IEEE Trans. Antennas Propag.*, vol. 61, no. 9, pp. 4588–4597, Sep. 2013, doi: 10.1109/TAP.2013.2264795.

ANTONIO J. RUBIO (Graduate Student Member, IEEE) graduated from Naval Nuclear Power Training Command Power School in 2011, and Naval Power Training Unit, Charleston, S.C. in 2012, before serving on the USS Providence (SSN-719). He received the B.S. degree in electrical engineering from Florida International University, Miami, FL, USA, in 2019, where he is currently pursuing the Ph.D. degree in electrical and computer engineering. He is currently serving as a Graduate Research Assistant with the Transforming Antennas Center, FIU. His research is focused on RF systems, communications, deployable and reconfigurable antennas, reflectarrays, and machine learning optimization.

ABDUL-SATTAR KADDOUR (Member, IEEE) received the first B.S. degree in electronics from the Faculty of Science, Lebanese University, Lebanon, in 2011, the second B.S. and M.S. degrees in electronics and embedded systems engineering from the Grenoble Institute of Technology, Grenoble, France, in 2012 and 2014, respectively, and the Ph.D. degree in optics and radiofrequency from Grenoble Alpes University, Grenoble, in 2018. His Ph.D. was realized with CEA-LETI, Grenoble, where he developed electrically small and frequency reconfigurable antennas for space applications. In 2018, he joined the Xlim Research Institute, Limoges, France. From 2019 to 2022, he has been a Research Fellow with Transforming Antennas Center, Florida International University, Miami, FL, USA. Since 2022, he has been an Antenna Communication Engineer with Teltrium. He has four issued patents in the U.S. Patent Office. His main research interests include electrically small antennas, reconfigurable antennas, antenna arrays, reflectarrays, and wireless power transfer systems. He serves as a Reviewer for the numerous IEEE journals in the field of Microwave, Antennas and Propagation.
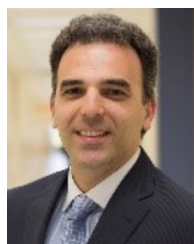
STAVROS V. GEORGAKOPOULOS (Senior Member, IEEE) received the Diploma degree in electrical engineering from the University of Patras, Patras, Greece, in June 1996, and the M.S. and Ph.D. degrees in electrical engineering from Arizona State University, Tempe, AZ, USA, in 1998 and 2001, respectively. From 2001 to 2007, he was the Principal Engineer with SV Microwave, Inc. Since 2007, he has been with the Department of Electrical and Computer Engineering, Florida International University, Miami, FL, USA, where he is currently a Professor, the Director of Transforming Antennas Center (a research center on foldable/origami, physically reconfigurable and deployable antennas), and the Director of the RF Communications, Millimeter-Waves, and Terahertz Lab. His current research interests relate to novel antennas, arrays, RFID, microwave and RF systems, novel sensors and wireless powering of portable, as well as wearable and implantable devices. He received the 2015 FIU President's Council Worlds Ahead Faculty Award, which is the highest honor FIU extends to a Faculty Member for excelling in research, teaching, mentorship, and service. He served as an Associate Editor of the IEEE TRANSACTIONS ON ANTENNAS AND PROPAGATION from 2013 to 2019 and has been serving as an Associate Editor of the IEEE OPEN JOURNAL OF ANTENNAS AND PROPAGATION since 2019.